Synoptic-Scale Features Associated with Warm Season Heavy Rainfall over the Interior Southeastern United States

CHARLES E. KONRAD II

Department of Geography, University of North Carolina at Chapel Hill, Chapel Hill, North Carolina

(Manuscript received 1 July 1996, in final form 29 April 1997)

ABSTRACT

Previous research has established links between heavy rainfall and a wide variety of synoptic features and parameters. In this study, 312 heavy rainfall events are identified over the southeastern United States and used to construct a synoptic climatology that relates 14 synoptic features and parameters to the occurrence and amounts of heavy rainfall. To carry this out, an automated synoptic typing scheme is employed to classify the heavy rainfall sample according to several characteristics of the synoptic regime. This classification provides five distinct synoptic patterns that can be associated with heavy rainfall over the southeastern United States. Commonly occurring synoptic features in each synoptic pattern are highlighted and discussed. Correlation analysis is then used to relate the occurrence and strength of these features to the heavy precipitation totals.

Heavy rainfall in four out of the five identified synoptic patterns is most frequently associated with high levels of moisture at the 700-mb level. Ridging in the 850-mb warm air advection field is common over the heavy rain area as well. Numerous relationships are identified between the heavy rainfall amounts and the character of synoptic features; however, the nature of these relationships is found to vary strongly according to the synoptic pattern.

1. Introduction

Previous heavy rainfall studies have identified numerous patterns and mechanisms on the synoptic and mesoscale that are connected with or promote heavy rain development. Case study analyses (e.g., Bosart and Carr 1978; Schwartz et al. 1990) have provided detailed information on the evolution of the storm environment during extremely heavy rainfall events. In addition, synoptic climatological studies have revealed suites of atmospheric features (i.e., scenarios) that are typically associated with extremely heavy rain events (e.g., Winkler 1988) or flooding episodes (e.g., Maddox et al. 1979). Although these studies collectively identify a range of synoptic conditions and environments than can be associated with extremely heavy rainfall, it is not clearly known what climatological relationships exist between the character of these features and the amounts of the heavy rainfall. Without knowledge of these relationships, it is tacitly assumed that these features, when occurring together in some combination, are diagnostic of extreme precipitation. A need exists, therefore, to distinguish between the synoptic environments associated with extremely heavy precipitation events that have the potential to produce flash flooding from those environments connected with ordinary events in which the flooding potential is much less.

In this study, a synoptic climatology of heavy rainfall was developed from a sample of 312 events over the interior southeastern United States. The precipitation totals were statistically related to the occurrence and magnitude of various synoptic-scale features previously shown to be associated with heavy rainfall. Since heavy precipitation can be observed in a variety of synoptic environments (e.g., Maddox et al. 1979; Doswell et al. 1996), the study sample was first classified objectively into groups on the basis of the associated synoptic pattern, and statistical relationships were developed between precipitation totals and various synoptic characteristics for each group.

2. Synoptic-scale features previously tied to heavy rainfall

It is well known that convective cells develop and interact with one another on the mesoscale (10–100 km) in ways that can promote heavy rainfall (Chappell 1986). These convective cell interactions typically occur within a synoptic- (or subsynoptic-) scale (100–1000 km) environment in which various thermodynamic parameters (e.g., temperature and moisture) exhibit high values. For example, high values of precipitable water (e.g., Hoxit et al. 1978; Korty 1980; Schwartz et al. 1990), instability (Bosart and Carr 1978; Maddox et al.

Corresponding author address: Dr. Charles E. Konrad II, Department of Geography, University of North Carolina at Chapel Hill, 203 Saunders Hall, CB#3220, Chapel Hill, NC 27599-3220.
E-mail: konrad@geog.unc.edu

1979; Funk 1991), and lower-tropospheric moisture (e.g., Grice and Maddox 1983; Winkler 1988) have been associated with heavy rainfall. Additionally, heavy rainfall has been connected with large values of positive equivalent potential temperature (θ_e) and moisture advection in the lower troposphere (Maddox et al. 1979; Winkler 1988; Konrad and Meentemeyer 1994). Also, Maddox and Doswell (1982) have tied intense convection, which is often associated with heavy rainfall, to lower-tropospheric warm air advection.

Numerous studies have noted the occurrence of synoptic-scale features that encourage dynamic lifting in the vicinity of heavy rain events. In the quasigeostrophic omega equation (Holton 1979), various forcings (e.g., positive differential vorticity advection, diabatic heating, and the Laplacian of warm air advection) promote rising air motions. Positive differential vorticity advection, which is usually found immediately upstream of a middle-tropospheric trough, has been tied indirectly to heavy rainfall. For example, Maddox et al. (1979) in his synoptic- and frontal-type events identified a middle-tropospheric shortwave immediately upstream of the heavy rain area. Many other studies, including Giordano and Fritsch (1983) and Winkler (1988), have documented the presence of weak 500-mb shortwave troughs upstream or in the immediate vicinity of the heavy rain region. Heavy rainfall is also promoted in the vicinity of fronts where low-level convergence forces the ascent of air displaying high levels of θ_e. Belville and Goetsch (1983), Funk (1991), and Wilson (1992), for example, have tied the low-level convergence associated with frontal boundaries to heavy rainfall. More recently, dynamic uplift forced by upper-tropospheric jet streaks has received attention in the literature (e.g., Ma and Bosart 1990; Funk 1991).

Numerous studies suggest that heavy rainfall occurs frequently near a ridge feature found in various thermodynamic fields. Although the absolute value (i.e., magnitude) of the thermodynamic field may not be especially strong in the vicinity of a ridge, the magnitudes are sufficiently greater than those found in surrounding areas to favor the instigation of convection and thus increase the potential for heavy rainfall. Maddox et al. (1979), for example, identified an 850-mb moisture ridge in three of their heavy rain types. Reynolds (1992), Wilson (1992), and other case studies of heavy rain documented the presence of moisture ridges at 850 mb and other levels in the atmosphere. Moreover, Grice and Ely (1983) recommended using the 850-mb moisture ridge in predicting the region of heaviest rainfall. Funk (1991) found that convection develops frequently in the vicinity of an 850-mb θ_e ridge where instability and a lifting mechanism are present. Finally, Konrad and Meentemeyer (1994) showed that numerous heavy rain events occur near or immediately downstream of a region in which the local maxima of 850-mb thermal advection (i.e., ridge) intersect an area of relatively unstable air. Although it has not been stated explicitly, heavy rain events may be connected with ridges or troughs present in synoptic fields that promote forced or dynamic uplift (e.g., boundary layer convergence and positive vorticity advection). Although the term ''ridging'' is used rarely in the description of these fields, it is certainly applicable.

Because of the number of synoptic-scale features and patterns known to be associated with heavy rain, the forecasting of the general location of heavy rainfall on any given day presents a tremendous challenge. According to Funk (1991), the National Centers for Environmental Prediction analyzes various model output and at least eight fields in the prediction of heavy rainfall. Additionally, at least seven ''rules of thumb'' are employed to interpret these fields. Because warm season heavy rainfall occurs primarily on the mesoscale within a quiescent synoptic environment, various subtle features on the synoptic scale can encourage convection and heavy rainfall. Indeed many heavy rain events, such as the mesohigh-type events identified by Maddox et al. (1979), may not be strongly associated with any well-defined synoptic-scale feature.

Given the variety of synoptic situations and features that have been tied to heavy precipitation, it is important to isolate those features whose presence or strength may distinguish ordinary heavy rainfall events from extremely heavy events. In this study, the character of these synoptic features is related to heavy precipitation totals.

3. Methodology

a. Heavy rain archive

The hourly precipitation dataset (HPD) for a network of stations within the interior southeastern United States (Fig. 1) were acquired to develop a heavy rain archive for the study. HPD were examined for nine warm seasons (1 May–30 September) within the period 1 May 1982–30 June 1990 to identify heavy rain events. Precipitation events were defined in this study by the occurrence of measurable precipitation for a period in which breaks in the precipitation did not exceed 2 h. If at least 5 cm of precipitation were observed at one or more HPD stations within a 6-h period, the event was defined as heavy. Using this definition, 312 events were identified. Various attributes of the heavy rain, including the hour of heaviest rainfall and the highest intensity of hourly rainfall, were documented at the HPD station receiving the heaviest precipitation during each given 24-h period (1200 to 1200 LST) of the study period. If two HPD stations received over 5 cm of precipitation and a time separation of 12 h or more was observed in the hour of heaviest rainfall, information from both HPD stations was recorded in the heavy rain archive as two separate events. If heavier rainfall amounts were identified at any HPD stations 200 km or less outside the study area during the 24-h period, the event was not archived.

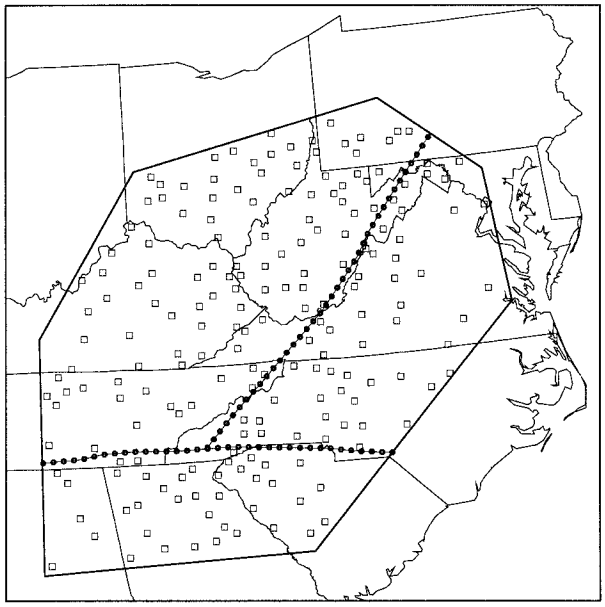

FIG. 1. The study area. Squares denote HPD stations used to build the heavy rain archive. The dotted lines separate the eastern, southern, and western regions of the study area.

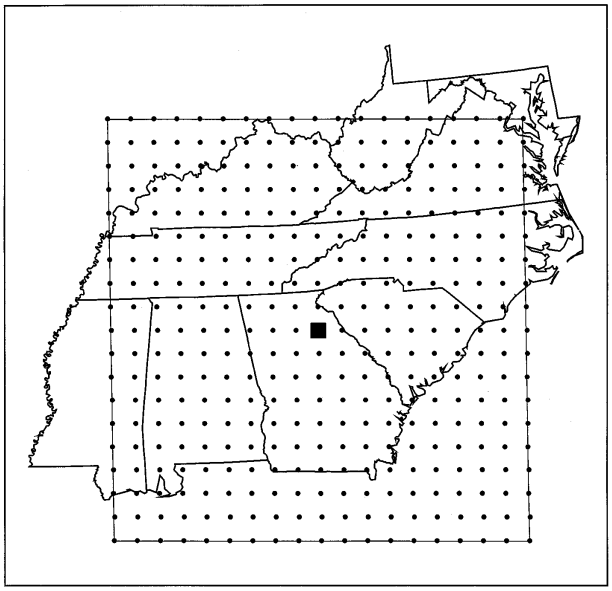

FIG. 2. Example of the use of a floating grid for a hypothetical heavy rain event in northeast Georgia (square). Synoptic field magnitudes were estimated at each grid point (circle).

b. Synoptic fields

To identify features in the synoptic environment associated with each heavy rain episode, gridded (190 km by 190 km), twice-daily synoptic data from the initialized fields of the Limited-Area Fine Mesh (LFM) model provided by the National Center for Atmospheric Research were spatially interpolated onto a 1000 km × 1000 km floating grid (grid interval 55.5 km) centered over the estimated location of heaviest precipitation (see Fig. 2 for an example). An inverse distance technique in which the influence of LFM data points declines exponentially with distance was used to carry out the interpolation. Only the four nearest LFM grid points were used in the technique to interpolate a given field value. The grid size and resolution were chosen to provide a sufficiently large region to capture synoptic-scale features and, at the same time, allow a fine enough mesh for a reasonable estimate of the locations of field maxima and ridging axes. Obviously, this spatial interpolation will not reveal mesoscale features whose resolution is beneath the scale of the raw data.

The synoptic data included wind (u and v components), temperature, and height at the standard pressure levels as well as dewpoint temperature at most levels and precipitable water. Because of the desire to base the climatology on the atmospheric conditions immediately prior to the onset of the heavy rainfall, a linear interpolation scheme was employed to estimate gridpoint values in each field for the period immediately prior to the onset of heavy rainfall. Using the 0000 and 1200 UTC gridded synoptic fields, the linear interpolation scheme estimated field point values for the map time 2 h prior to the hour of heaviest rainfall. For example, if an event exhibited the heaviest rainfall at 0600 UTC, field values from the 0000 and 1200 UTC gridded fields would be utilized to estimate gridded field values in the vicinity of the event at 0400 UTC.

Using the gridded synoptic dataset, atmospheric fields associated with 13 features previously connected with heavy rainfall were accessed or calculated from the gridded synoptic dataset (Table 1). Note that the 14th feature in Table 1, the diurnal timing of the event, was obtained from the HPD data. Various thermodynamic and moisture fields, including equivalent potential temperature (θ_e) and mixing ratio, were calculated at several levels in the troposphere. Precipitable water, which provides a measure of the water vapor contents integrated through the depth of the troposphere, was accessed directly from the LFM dataset. Because of its usefulness in assessing moisture availability and depth in the atmosphere (Funk 1991), the K index was used to estimate airmass instability. Because the LFM dataset was restricted to the standard levels of the raowinsonde profile, other stability indices, particularly those less biased toward moisture, could not be calculated. But by using SHARP software and the CD *Radiosonde Data of North America (1946–1992)* published by the National Climate Data Center (1993), point values of the lifted, Showalter, and total totals indices as well as positive convective available potential energy (CAPE) values were estimated over the location receiving the heaviest rainfall. Finally, the related fields of 850-mb θ_e and warm air advection were calculated in this work since both have been associated with heavy precipitation.

Synoptic features associated with dynamic uplift in

TABLE 1. Features associated with heavy rainfall and the atmospheric fields (event characteristics) used to assess the strength (character) of these features.

Feature associated with heavy rainfall	Atmospheric field or event characteristic
1) Low and midlevel moisture	850-mb mixing ratio 700-mb mixing ratio 500-mb mixing ratio Precipitable water
2) Thermodynamic energy	850-mb θ_e 700-mb θ_e 500-mb θ_e
3) Instability	K index Lifted index Showalter Total totals CAPE (+)
4) Surface warm air	Surface temperature
5) Moisture and warm air advection	850-mb θ_e advection 850-mb warm air advection
6) Low-level moisture convergence	850-mb θ_e divergence
7) Low-level convergence	Boundary layer divergence
8) Upper-level divergence	200-mb divergence
9) Midlevel positive vorticity advection	500-mb vorticity advection
10) Midlevel vorticity minimum and maximum	500-mb vorticity
11) Slow convective cell steering winds	Magnitude of 850–200-mb vector wind
12) Southerly to southeasterly convective cell steering winds	Direction of 850–200-mb vector wind
13) Lower-tropospheric wind veering	Degree of offset between convective cell steering and boundary layer winds
14) Diurnal timing of events with nocturnal and early morning events favoring heavy rain	Timing of the hour of heaviest precipitation

heavy rain events were calculated including boundary layer convergence, 200-mb divergence, and differential positive vorticity advection (PVA), which is approximated by PVA at the 500-mb level. It should be noted that the boundary layer convergence was estimated over a synoptic scale; therefore, regions of mesoscale convergence connected with thunderstorm outflow boundaries were not identified. Vorticity at the 500-mb level was calculated in order to identify regions of minimum vorticity (i.e., 500-mb ridge lines) relative to the location of heaviest rainfall. Maddox et al. (1979), Winkler (1988), and Funk (1991) have connected various types of heavy rain events to the close positioning of a 500-mb longwave ridge. Also, regions of maximum vorticity (500-mb trough axes) were identified as well because of connections observed between weak 500-mb waves and convection in some heavy rain events. To estimate 850-mb thermal and θ_e advection, θ_e divergence, boundary layer divergence, 500-mb vorticity and vorticity advection, a center differencing scheme was employed [see Konrad and Colucci (1989) for details]. The θ_e convergence was estimated by computing 850-mb convergence using center differencing and multiplying the result by the scalar θ_e.

Heavy rainfall may be connected with a single or series of convective cells that move slowly over a local area in response to weak tropospheric winds. To assess the speed and movement of convective cells, a mean 850–200-mb wind was estimated by calculating the magnitude and direction of the vector mean wind from the 850-, 700-, 500-, and 200-mb level wind vectors. Newton and Fankhauser (1975) and others have estimated this wind in a similar manner. The veering of the wind below 2.5 km has also been associated with heavy rainfall (Opitz et al. 1995). To provide a measure of lower-tropospheric wind veering, the directional difference (or shear) between the mean 850–300-mb-layer wind and boundary layer winds was computed. Finally, the timing of each heavy rain event was noted. Crysler et al. (1982) and Winkler (1987) found that extremely heavy rainfall exhibits an evening or nocturnal maximum in occurrence during the summer; on the other hand, lighter events display a maximum in the late afternoon.

Since heavy rainfall has been connected with the occurrence of ridges in various synoptic fields, ridge positions were estimated in all of the synoptic fields. The presence or absence of a ridge feature was noted in a circular region within 112 km of the location of heaviest rainfall in each event. A categorical variable for each synoptic field was assigned one of two values (no ridging = 0, ridging = 1) based on the presence or absence of a ridging feature. Ridge positions on the floating grid were defined by the set of grid points exhibiting the highest values in each north–south and east–west traverse across the floating grid as shown by the example in Fig. 3. Although the east–west and north–south traverses were limited to two orientations, the identified set of field maxima provided good estimates of ridges oriented in any direction. The automated technique was checked in a random sample of events to ensure that the ridge positions were estimated accurately. Although the technique appears to be accurate in identifying ridges on a synoptic scale, it may be considered suspect in identifying subsynoptic-scale ridges that cannot be discerned on the initialized LFM dataset, especially in data-sparse regions such as the Gulf of Mexico. The interest of this study, however, is simply to identify the presence or absence of synoptic-scale ridges within 112 km of the heavy rain event.

c. Synoptic classification

The relationship between the nature of a given atmospheric feature and the heavy rain totals was assumed

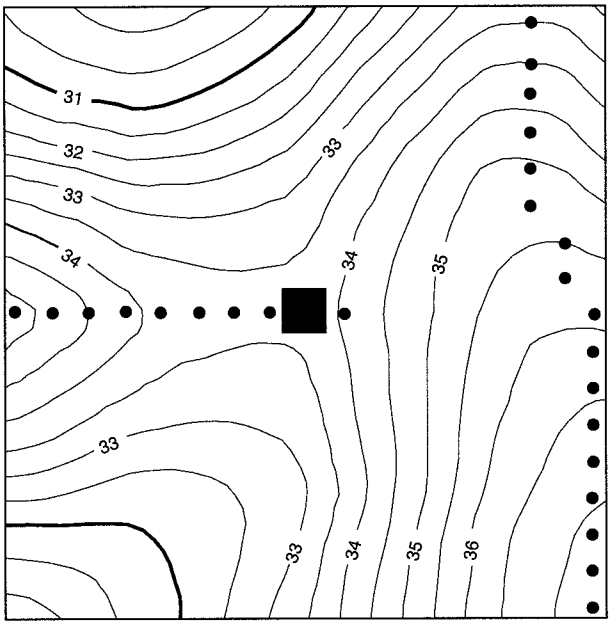

FIG. 3. Example of the use of the ridge identification technique. The solid lines denote key contours of instability as estimated by the *K* index. Closed circles provide the ridge axis positions as estimated by the technique. Note that the technique was used only to note the presence or absence of ridges within 112 km of the grid center (solid square).

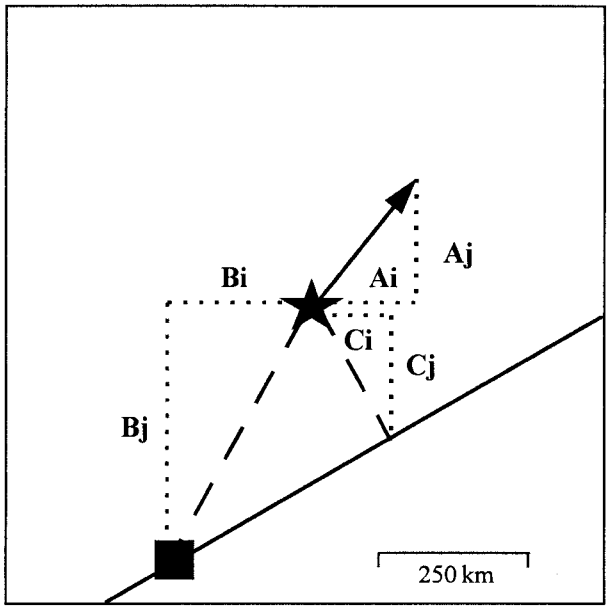

FIG. 4. Example of the three vectors used to classify the synoptic environments associated with the heavy rain sample. The solid line provides the location of the nearest boundary layer convergence ridge (i.e., front), and the square displays the location of greatest boundary layer convergence (i.e., typically a surface low pressure wave). The arrow identifies the 500-mb wind vector (**A**). The dashed lines provide vectors from the location of heaviest rainfall (star) to the location of greatest boundary layer convergence (**B**) and the nearest ridging location of boundary layer convergence (**C**). The *u* and *v* components of the three vectors (*Ai*, *Aj*, *Bi*, *Bj*, *Ci*, *Cj*) are used as input variables for the cluster analysis.

to vary according to the synoptic situation in this work. For example, any relationship identified between surface temperature and heavy rainfall totals will depend to some degree on whether or not the heavy rain is observed in the cool or warm sector of a cyclone. Woodcock (1980) has shown that relationships between predictors and predictands in analog weather forecasts vary from one synoptic pattern to the next. Moreover, he demonstrated that the relationships were stronger when the samples used to establish the relationships were collected from similar synoptic situations. Given the variety of synoptic situations in which heavy rainfall can be observed (e.g., Maddox et al. 1979; Heideman and Fritsch 1988; Winkler 1988), it is useful to classify the heavy rain samples into groups on the basis of these synoptic situations and to identify statistical relationships within each group.

Six variables were used as input variables for a cluster analysis to assign heavy event into groups or clusters on the basis of similarities in the synoptic pattern. A cursory examination of a portion of the study sample revealed that synoptic variability is most marked in the lower troposphere and relates to the position of fronts and low pressure centers in the lower troposphere. Therefore, four of out of the six input variables were designed to identify the position of the nearest front and center of low pressure. Since these features are typically weak during the warm season, they may be best expressed by the synoptic-scale pattern of boundary layer convergence (BLC). As shown in Fig. 4, the four input variables consist of the i and j components of two vectors (**B** and **C**), the first of which extends from the location of heaviest rainfall to the area of greatest BLC or low pressure center (variables *Bi* and *Bj*) and the second of which projects to the nearest ridge of BLC or front (variables *Ci* and *Cj*). The remaining two variables (*Ai* and *Aj*) provide the 500-mb wind vector and thus a basic characterization of the middle-tropospheric flow near the heavy rain event. Less emphasis (i.e., only two of the six input variables) is placed on this circulation because the synoptic variability at this level is not as pronounced; in particular, many events display a strong southerly component.

To carry out the classification in an objective and automated fashion, a two-step cluster analysis procedure described by Stooksbury and Michaels (1991) and Davis and Rogers (1992) was performed in this work. First the six input variables were used in an average linkage clustering procedure. This hierarchical technique merges or clusters individual events that are most alike and continues merging individuals, or groups of individuals already clustered together, that are progressively less alike until a single large group is obtained. Using the pseudo-F statistic (SAS Institute 1988) as a guide, a subjective choice was made as to the optimal point in the merging process in which reasonably different clus-

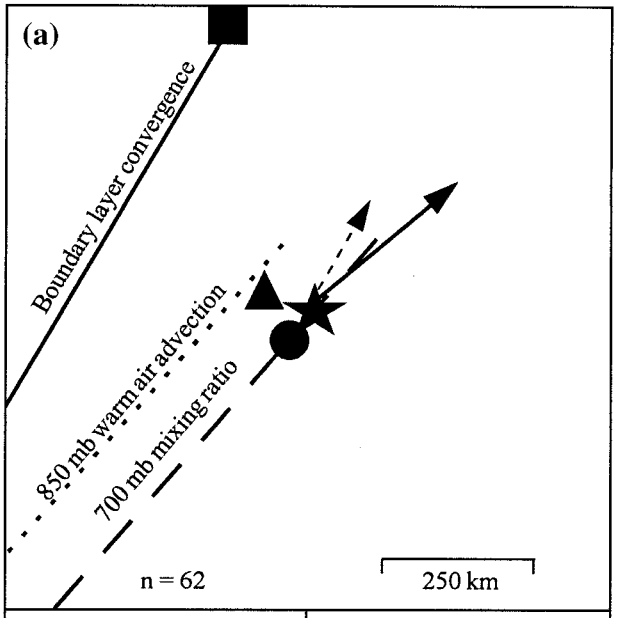

Field	Ridging (%)
K-index	71
850 mb warm adv.	68
700 mb mixing ratio	67
850 mb mixing ratio	66
700 mb theta-e	64
850 mb theta-e adv.	64
850 mb theta-e	60
500 mb PVA	54

Field	Mean magnitude
700 mb mixing ratio	0.52
K-index	0.49
850 mb mixing ratio	0.41
700 mb theta-e	0.39
850 mb warm adv.	0.37
850 mb theta-e adv.	0.36
850 mb theta-e	0.33

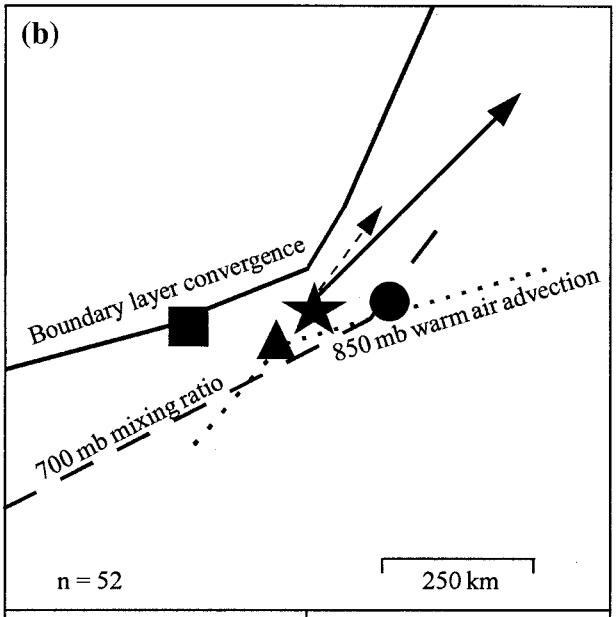

Field	Ridging (%)
700 mb mixing ratio	69
850 mb warm adv.	64
Boundary lyr. conv.	63
850 mb theta-e conv.	63
K-index	61
850 mb mixing ratio	58
700 mb theta-e	57
500 mb PVA	56
850 mb theta-e adv.	50

Field	Mean magnitude
Boundary lyr. conv.	0.55
700 mb mixing ratio	0.53
K-index	0.51
200 mb divergence	0.50
850 mb mixing ratio	0.43
700 mb theta-e	0.43
850 mb warm adv.	0.40
850 mb theta-e adv.	0.37

FIG. 5. Schematic map depicting the most frequently occurring positions of various features in synoptic patterns 1 through 5 (a) through (e). The most common positions of greatest boundary layer convergence, 700-mb mixing ratio, and 850-mb warm air advection are denoted by the square, circle, and triangle, respectively. The most common ridging locations of boundary layer convergence, 700-mb mixing ratio, and 850-mb warm air advection are delineated by the solid, dashed, and dotted lines, respectively. The thick, solid arrow provides the mean 850–200-mb wind vector, and the thin, dashed arrow shows the mean boundary layer wind vector. The length of these arrows is proportional to the magnitude of the wind vectors. The bottom-left panel displays all fields in which a ridge is observed within 112 km of the location of heaviest rainfall. The bottom-right panel specifies all fields in which the mean normalized field magnitude over the location of heaviest rainfall exceeds 0.30 Z (0.30 standard deviations above normal relative to other gridpoint values in the sample).

ters remained. In this study, this point was reached with five clusters remaining. Cluster centroids (averages) were then computed for each group. In the second step, each centroid served as a cluster seed value for convergent *k*-means clustering, a nonhierarchical technique. In this approach, each heavy rain event was reassigned membership to the cluster displaying the nearest seed value. After all events were reassigned, a new seed value was calculated for each cluster. The process of cluster reassignment and cluster seed recalculation was repeated until the change in seed values between interations fell below a preselected amount (0.001 in this study). This cluster analysis approach provided five distinct synoptic patterns as shown by the composite patterns of boundary layer convergence ridging (i.e., fronts) in Figs. 5a–e. The 500-mb wind vectors (note that the mean 850–200-mb wind vector in Figs. 5a–e provides a close approximation) show less variability between patterns, but this is to be expected since this vector displayed much less variability (i.e., see earlier

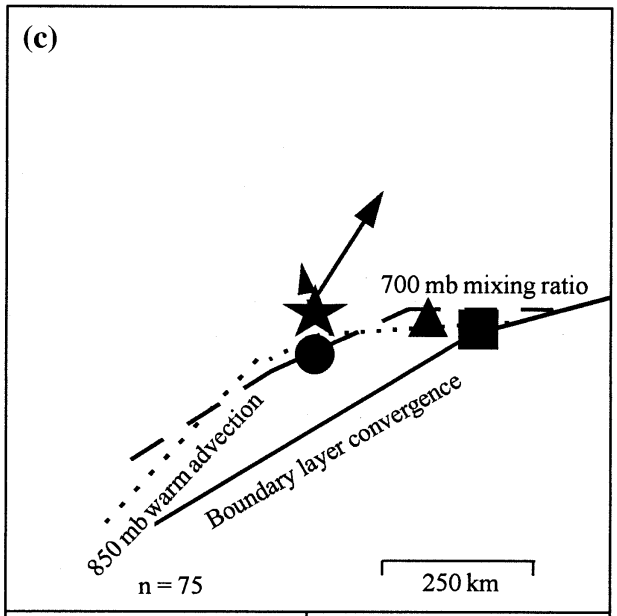

Field	Ridging (%)
700 mixing ratio	64
K-index	60
850 mb mixing ratio	57
200 mb divergence	52
850 mb warm adv.	50

Field	Mean magnitude
700 mixing ratio	0.42
K-index	0.42
700 mb theta-e	0.31
850 mb mixing ratio	0.30

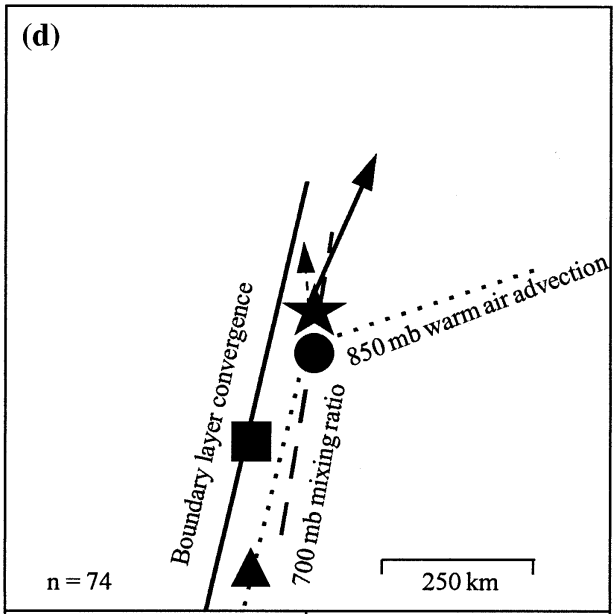

Field	Ridging (%)
700 mb mixing ratio	61
Boundary lyr. conv.	58
700 mb theta-e	54
850 mb mixing ratio	53
850 mb warm adv.	53
K-index	51
850 mb theta-e conv.	50

Field	Mean magnitude
700 mb mixing ratio	0.45
K-index	0.39
700 mb theta-e	0.35
850 mb mixing ratio	0.33

FIG. 5. (*Continued*)

discussion) and was given a weaker weighting in the clustering scheme.

Before identifying the relationships between the synoptic features and the heavy rainfall totals, it is useful to compare the absolute value (i.e., magnitude) of the synoptic fields over the location receiving the heaviest rainfall with the field magnitudes found in the surrounding region (i.e., remaining portions of the floating grid). The magnitude of this difference can be used to assess the degree to which high field magnitudes correspond with the location of heaviest rainfall. To assess this difference, the synoptic field values associated with each event were normalized with respect to the field values observed over the entire floating grid in each of the five synoptic situations. The fields were normalized by subtracting the field mean obtained for each cluster and dividing by the field standard deviation. The normalized field values over the location of heaviest rainfall, therefore, provide a measure of the relative correspondence of this location with high or low field magnitudes in a given synoptic field. Also, normalized values provide a means for comparing magnitudes of different synoptic field variables over the location of heaviest rainfall.

To assess relationships between various synoptic field features and the totals of heavy precipitation, a correlation analysis was performed. Both the magnitude of the synoptic field and the presence or absence of a ridging feature (categorical variable) were correlated with the heavy precipitation totals for the sample of heavy rain events associated with each synoptic pattern. Only correlations that are statistically significant at the 0.05 level are reported in this paper. The strength of the re-

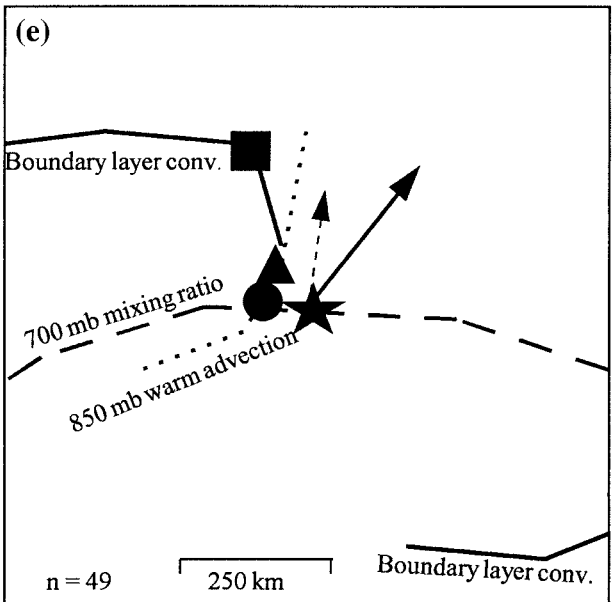

Field	Ridging (%)
700 mb mixing ratio	71
850 mb warm adv.	68
K-index	67
850 mb mixing ratio	63
700 mb theta-e	61
850 mb theta-e adv.	50
500 mb theta-e	55
500 mb PVA	53

Field	Mean magnitude
700 mb mixing ratio	0.58
K-index	0.52
700 mb theta-e	0.44
850 mb mixing ratio	0.42
850 mb theta-e adv.	0.39
850 mb theta-e	0.34
850 mb warm adv.	0.28

FIG. 5. (*Continued*)

lationships identified by correlation bears some dependence on the range of the dependent and independent variables in a statistical sample. Reductions in the range of one or both of the variables often results in a lowering of the correlation coefficient. The range of precipitation totals, the dependent variable in this study, was restricted to amounts exceeding 5 cm. Therefore, the correlations with the synoptic field characteristics were more modest. By restricting the study sample to heavy rainfall events, however, attention was focused on synoptic field differences between ordinary and extremely heavy rainfall events.

d. Orographic influences

Heavy rainfall in this study is affected by the southern Appalachian highlands, which consist of the Blue Ridge

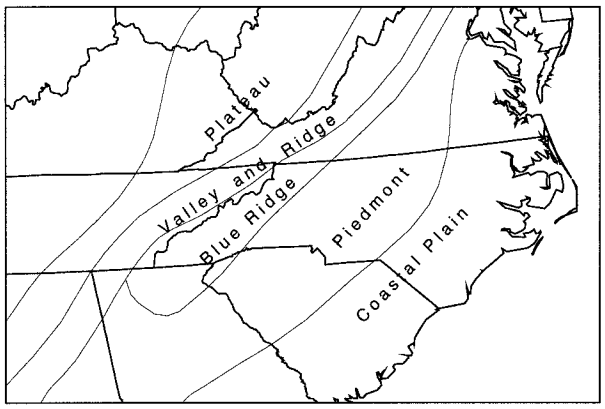

FIG. 6. Physiographic regions found in the study area.

Mountains (1000–2000 m), the valley, and ridge (600–1400 m), as well as the adjacent upland Piedmont (100–300 m) and plateau (300–950 m) (Fig. 6). Although warm season heavy rainfall frequencies are greatest toward the Atlantic coast (Fig. 7), the mountain range may be tied to a region of higher frequencies (greater than 1.2 events yr^{-1}) extending along southeastern slopes of the Blue Ridge Mountains and the upper Piedmont. The interior and northwestern portions of the Appalachians, on the other hand, lie in a rainshadow for heavy events with seasonal rates that are markedly lower than those found on the southeastern slopes. In a trajectory analysis of the moisture-bearing circulations over the Appalachians, Konrad (1994) showed that the southeastern slopes of the Blue Ridge Mountains and adjacent Piedmont generally experience heavy rainfall when southeasterly to southerly winds promote orographic uplift and moisture advection from the eastern gulf and Atlantic coasts. Alternatively, heavy rainfall on the northwestern slopes and adjacent plateau regions,

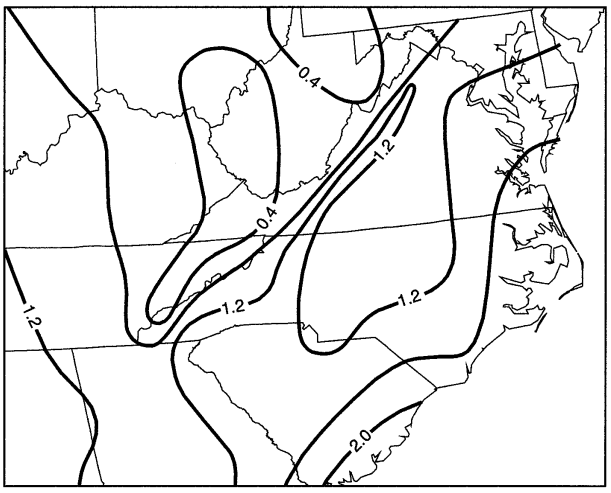

FIG. 7. Mean warm season frequencies of heavy rainfall (event totals exceed 5 cm) computed from HPD data for the period 1948–88.

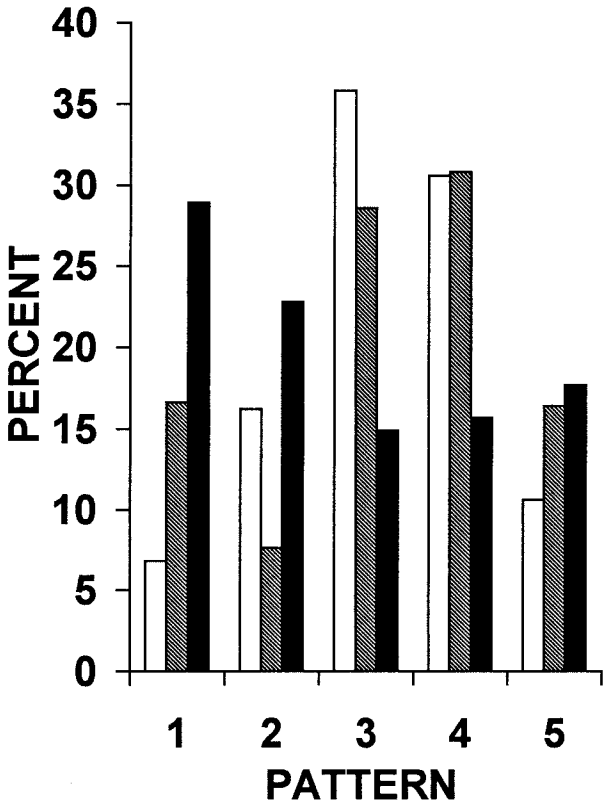

FIG. 8. Percent of events in the eastern (unshaded), southern (stripped), and western (shaded) regions that are associated with each synoptic pattern.

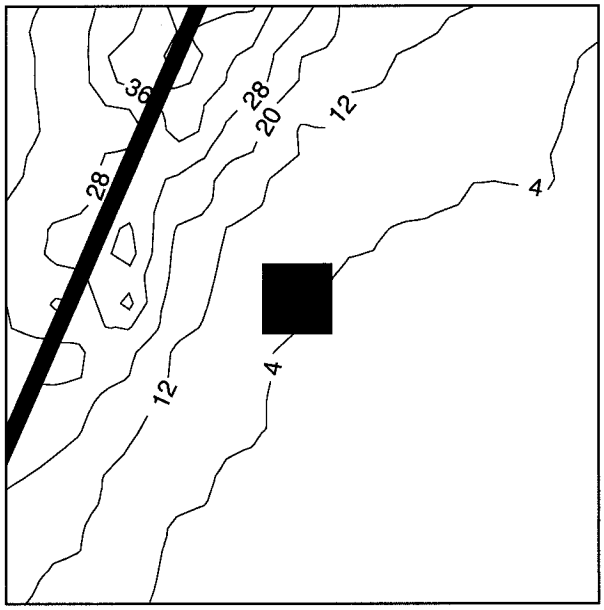

FIG. 9. Composite of boundary layer convergence ridging frequencies (i.e., frontal positions) for pattern 1. The thick line approximates the position of the composite ridge axis and appears on the schematic map (Fig. 5a).

while less common, was tied to southwesterly or westerly winds that advect moisture from the lower Mississippi River Valley or the western Gulf of Mexico.

In order to relate the influence of the Appalachian highlands to the five identified synoptic patterns of heavy rainfall, the study area (Fig. 1) was subdivided into three regions (eastern, southern, and western) on the basis of the boundary layer wind directions that are most strongly tied to heavy rainfall (i.e., southeasterly, southeasterly to southwesterly, and southwesterly winds in the eastern, southern, and western regions, respectively). For each region, membership in the five synoptic pattern groups was noted (Fig. 8), and thus the synoptic patterns that commonly produce heavy rainfall in each region could be identified.

4. Results

To portray commonly occurring features in each of the five synoptic patterns (clusters), field composites were developed. These composites were originally constructed in the usual way by simply calculating mean fields for each cluster; however, the observed features in these composites were found in many cases to be influenced strongly by high-magnitude field values contained in a small number of events of the sample. Thus, various weakly defined synoptic features (e.g., fronts and low pressure centers) were masked by the high magnitude fields in the remaining events. To ensure an equal representation of the features associated with each event, composite ridge positions, which are not affected by high field magnitudes, were used instead of the field means to portray the synoptic situation.

Schematic maps (Figs. 5a–e) illustrate the most frequent positioning of various synoptic features including, the location of fronts as inferred from composites of boundary layer convergence ridging (Fig. 9 provides an example). Several fields (e.g., moisture and warm air advection) showed consistently higher ridging frequencies in the vicinity of the location of heaviest rainfall. Therefore, the ridging locations and field maxima associated with these fields are provided on the schematic maps as well. Since the 700-mb mixing ratio field displayed the highest normalized magnitudes and frequencies of ridging near the heavy rain region, its position was plotted on the diagram as the best representative of the moisture field variables.

a. Pattern 1

The pattern 1 composite (Fig. 5a) displays a region of boundary layer convergence about 400 km northwest of the heavy rain location. This region may be connected with a low pressure center and trailing cold front to the southwest. Moisture and warm air are forced northeastward from the Gulf of Mexico due to a southwesterly circulation ahead of the front in the lower to middle troposphere. The moisture and warm air advection are

TABLE 2a. Summary of the relationships obtained between various features and heavy precipitation totals in pattern 1. Only relationships that are statistically significant at the 0.05 level are reported. The first and fourth quartiles refer to lightest and heaviest quarters of the precipitation events in the sample, respectively. Correlations associated with the variable, timing, were computed using the time difference between the indicated time and the hour of heaviest rainfall. A negative correlation, therefore, shows the increased occurrence of heavier precipitation during the indicated period of the diurnal cycle (e.g., 0200 LST in pattern 1). Correlations connected with the variable, degree of veering, were calculated using an offset between the indicated degree of veering (e.g., 80° in pattern 1) and the observed degree of veering; thus, the negative correlation in this pattern indicates the occurrence of heavier precipitation with increasing veering up to the indicated value.

Field magnitude			
		Mean normalized magnitude	
Feature	Correlation	1st	4th quartile
500-mb θ_e	0.21	−0.15	0.57
Precipitable water	0.18	−0.23	0.42
Surface temperature	0.15	−0.59	0.01
Ridge presence/absence			
		Percent occurrence	
Surface temperature	0.51	0	31
Other features			
		Mean (degrees)	
Timing (0200 LST)	−0.24	—	—
Degree of veering (80°)	−0.18	21	27

greatest near the location of heaviest rainfall (composite center) as evidenced by the positioning of the warm air advection and mixing ratio ridges. The composite reveals that these ridges are typically located immediately upstream of the event and most frequently trended to the southwest–northeast. This trend is nearly parallel to the mean 850–200-mb wind vector and suggests that the convective cells responsible for the precipitation moved along these ridge axes. An instability ridge is found near the grid center in over 70% of the events. The mixing ratio and instability fields display the greatest normalized magnitudes over the grid center as shown in the lower-right panel of Fig. 5a. Finally, the pattern 1 events (Table 3) are nearly evenly distributed across the warm season.

Almost 30% of the events observed in the western region were connected with pattern 1 (Fig. 8), approximately 10% greater than what would be expected from a sample uniformly distributed across the five patterns. This contrasts with the southern and eastern regions where less than 17% and 7% are associated with this pattern, respectively. The increased occurrence of this pattern over the western region may be tied to the southwesterly circulation in the lower troposphere, which provides gulf moisture and upslope flow, especially over the western plateau.

Heavy rain totals in the cluster 1 events were most strongly related to the presence of a surface warm air ridge (Table 2a). This relationship is supported by the finding that none of the lighter events (first quartile sample) were connected with a warm air ridge, while 31% of the heavier precipitation events were associated with this ridge. Heavy rain totals were positively related to the field magnitudes of various thermodynamic fields including 500-mb θ_e, precipitable water, and surface temperature. Also, a significant association was found between the precipitation totals and the timing of the events with heavier events occurring with the greatest frequency during the early morning hours. Finally, precipitation totals was significantly correlated with the degree of veering in the lower troposphere.

TABLE 2b. Same as Table 2a except for pattern 2.

Field magnitude			
		Mean normalized magnitude	
Feature	Correlation	1st	4th quartile
850-mb warm air advection	0.43	0.24	0.87
850-mb θ_e convergence	0.32	0.47	0.58
500-mb θ_e	−0.26	0.22	−0.30
Surface temperature	−0.36	0.14	−0.52
Ridge presence/absence			
		Percent occurrence	
500-mb vorticity maximum	0.26	8	48
Boundary layer convergence	0.20	58	84
850-mb θ_e convergence	0.19	67	84
200-mb divergence	0.18	50	54
Other features			
Timing (0500 LST)	−0.19		

b. *Pattern 2*

The pattern 2 composite (Fig. 5b) depicts a region of boundary layer convergence immediately northwest of heavy rain location. An examination of the synoptic charts for 20 of the events revealed that this region was commonly tied to the existence of a slow-moving cold front with one or more centers of low pressure moving

TABLE 2c. Same as Table 2a except for pattern 3.

Field magnitude			
		Mean normalized magnitude	
Feature	Correlation	1st	4th quartile
850-mb θ_e convergence	0.26	−0.27	0.10
Boundary layer convergence	0.21	−0.37	0.03
500-mb vorticity	−0.15	0.44	−0.11
Ridge presence/absence			
		Percent occurrence	
500-mb vorticity minimum	0.21	33	52
Boundary layer convergence	0.16	33	37
Other features			
		Mean (degrees)	
Degree of veering (80°)	−0.21	−7	60
Timing (0000 LST)	−0.32		

TABLE 2d. Same as Table 2a except for pattern 4.

Feature	Correlation	Mean normalized magnitude 1st	Mean normalized magnitude 4th quartile
Field magnitude			
Precipitable water	0.26	−0.10	0.54
CAPE (+)	0.25	—	—
700-mb mixing ratio	0.25	0.19	0.78
850-mb mixing ratio	0.22	0.08	0.59
500-mb θ_e	0.22	0.01	0.55
700-mb θ_e	0.20	0.17	0.62
K index	0.15	0.25	0.56
500-mb PVA	−0.23	−0.14	−0.66
Surface temperature	−0.26	0.03	−0.46
Ridge presence/absence			
		Percent occurrence	
850-mb warm air advection	0.16	56	72
500-mb vorticity maximum	0.16	50	56
500-mb PVA	−0.22	56	33
Other features			
		Mean (°)	
Timing (0400 LST)	−0.37		
Mean 850–200-mb wind direction	−0.30	209	204
Degree of veering (55°)	−0.28	11	38

TABLE 2e. Same as Table 2a except for pattern 5.

Feature	Correlation	Mean normalized magnitude 1st	Mean normalized magnitude 4th quartile
Field magnitude			
Boundary layer convergence	0.35	−0.13	0.63
850-mb θ_e convergence	0.32	0.23	0.73
200-mb divergence	0.20	−0.19	0.16
Surface temperature	−0.24	−0.19	−0.40
Ridge presence/absence			
		Percent occurrence	
850-mb θ_e	−0.16	50	31
Precipitable water	−0.19	43	28
500-mb PVA	−0.21	64	54
Other features			
		Mean (°)	
Mean 850–200-mb wind direction	0.43	226	206
Timing (0200 LST)	−0.40		
Degree of veering (65°)	−0.30	15	35

along it. The mean 850–200-mb wind in this composite is markedly stronger (21 m s^{-1}) relative to the mean winds calculated in the other four synoptic patterns. Moisture and warm air advection ridges, which may be connected with strong southwesterly flow from the gulf coast region, are found most frequently in the vicinity of the pattern 2 events. The composite indicates that these ridges are most typically oriented from the heavy rain location to the west-southwest, a direction that nearly parallels the mean 850–200-mb wind. Nine fields display a ridging feature near the location of heaviest rainfall in 50% or more of the events. This includes features associated with dynamic uplift in the atmosphere (i.e., boundary layer convergence and 500-mb positive vorticity advection). Also, the normalized magnitudes of boundary layer convergence 700-mb mixing ratio, *K* index, and 200-mb divergence are quite high over the grid center. In fact, these magnitudes were greater than the vast majority of those found in the other four composite synoptic patterns. The pattern 2 events are most concentrated over the western region (Fig. 8). The southwesterly boundary layer winds associated with this pattern promote moisture and warm air advection from the gulf region to the exposed western plateaus and slopes. The pattern 2 events are observed most frequently during the early portion of the warm season (i.e., more than half of the sample was identified in May and June; Table 3), a period in which upper-air winds and synoptic-scale disturbances tend to be relatively stronger.

The synoptic pattern revealed in the pattern 2 composite bears a strong resemblance to the synoptic-type event defined by Maddox et al. (1979). Common features with the synoptic-type event include the occurrence of heavy rain in the warm sector near a relatively intense frontal system and/or cyclone, winds aloft nearly paralleling the front, high values of instability, and low-level moisture ridging with attendant warm air and moisture advection. Furthermore, the synoptic-type event may be connected with convective cells that repeatedly develop and move over the same general area in a ''train-echo'' pattern. The pattern 2 composite in this work indicates that the convective cells were steered (via the mean 850–200-mb wind) nearly parallel to the moisture and 850-mb warm air advection axes. Therefore, these ridging features may play a critical role in anchoring the convective system over the heavy rain area. To determine if this is the case, a mesoscale analysis of the pattern 2 events needs to be undertaken.

Heavy rainfall totals were most strongly associated with the magnitude of warm air and θ_e advection in pattern 2 (Table 2b). Significant positive relationships were also found with 500-mb vorticity ridging (i.e., 500-mb trough), boundary layer and 850-mb θ_e convergence ridging (indicative of a low-level front), and 200-mb divergence ridging. Heavy rain totals displayed negative correlations with surface temperature and 500-mb θ_e.

TABLE 3. Monthly frequencies of heavy rain events by pattern type.

Month	Pattern type 1	2	3	4	5
May	13	15	9	7	4
June	13	14	11	14	12
July	13	9	29	26	13
August	12	11	19	17	16
September	11	3	7	10	4

At first glance, this appears counterintuitive; however, many of the heavier events occurred during the transitional portion of the warm season when cooler surface temperatures and lower values of 500-mb θ_e would be expected. Finally, heavy rain totals were weakly correlated with the diurnal cycle as the heavier (lighter) events occurred with greater frequency during the early morning (late afternoon) hours.

c. Pattern 3

In the pattern 3 composite, a region of boundary layer convergence is found about 100 km southeast of the heavy rain location. An examination of the synoptic charts for 20 of the events revealed that this region was typically connected with a weak, stationary frontal boundary. The mean 850–200-mb winds are weaker (9.9 m s^{-1}) than those found in the other four pattern composites; this correlates with a midsummer peak in occurrence (i.e., nearly half of these events are observed in July and August; Table 3), a time when the synoptic-scale circulation is relatively weak. As seen in pattern 1 and 2 composites, 850-mb moisture and warm air advection ridges are situated near the location of heaviest rainfall. A moist southeasterly to southerly circulation induces frontal overrunning in many of the events. Unlike the first two patterns, the mean 850–200-mb wind is oriented at a slight angle with respect to the portrayed ridging features. Mean wind vectors computed in the mid- to upper levels of the troposphere (500–200 mb), however, are oriented nearly parallel to these ridge axes. Compared to the other patterns, relatively fewer fields display high magnitudes and ridging features in the vicinity of the event. Finally, the 700-mb mixing ratio and *K*-index fields showed the greatest magnitudes and frequencies of ridging near the event.

The pattern 3 synoptic composite resembles the frontal-type event identified by Maddox et al. (1979). Similarities include the occurrence of the heavy rainfall in the cool sector of a front, winds aloft (500-mb level and higher) nearly paralleling the front, and the occurrence of low-level warm air and θ_e advection over the frontal boundary and the heavy rain area. The front in these situations may serve as a focusing point for the convection and heavy rainfall as energy is provided by moisture and warm air advected northward from the gulf or Atlantic coast regions.

About 36% of the heavy rain sample over the Piedmont and eastern slopes were classified as pattern 3 events (Fig. 8); the southeasterly to southerly boundary layer circulation in this pattern provides moist upslope flow. The southern region also displays a relatively high concentration of pattern 3 events, but only about 15% of the western events are connected with pattern 3. The western plateau and slopes clearly lie in a rainshadow when the lower-tropospheric winds display a easterly component.

In the pattern 3 events, heavy rain totals were most strongly related to the timing of the precipitation as heavier (lighter) events occurred more frequently during the nocturnal (afternoon and early evening) hours (Table 2c). Significant positive correlations were also found with the magnitude of 850-mb θ_e and low-level convergence. This relationship suggests the increasing importance of a low-level frontal circulation near the more intense precipitation events. Also, a positive relationship was observed with low levels of vorticity and the presence of an axis of low vorticity values (i.e., 500-mb ridge). Finally, heavy rain totals was related to the degree of low-level wind veering, a variable that is highly correlated with a frontal circulation. The positive relationships obtained with the diurnal timing of the events and the low levels of vorticity coincide with Maddox et al.'s (1979) description of frontal events as being primarily nocturnal in nature and occurring near a 500-mb longwave ridge. (Note that Maddox et al.'s sample consisted of events that produced flooding and therefore may be considered extremely heavy.) Curiously, no significant relationships were uncovered between the precipitation totals and the magnitude of the moisture fields or the presence of a moisture ridge.

d. Pattern 4

The pattern 4 composite shows an elongated region of low-level convergence positioned from the location of heaviest rainfall south-southwestward to the southern grid boundary. This region was connected with the movement of a low pressure center north-northeastward from the Gulf of Mexico (in some cases along a slow-moving or stationary front). In some of the events, an east–west-oriented warm front was positioned 100–300 km south of the heavy rain area. Immediately east of the region of boundary layer convergence, the composite depicts the frequent positioning of a moisture and 850-mb warm air advection ridge. These features are tied to a southerly circulation immediately east of the approaching low pressure wave. As seen in patterns 1 and 2, these ridges are oriented nearly parallel to the boundary layer convergence region and the mean 850–200-mb wind. Moisture and boundary layer convergence ridging were observed most frequently in the vicinity of the pattern 4 events. With exception to the 700-mb mixing ratio, the normalized magnitudes of the other synoptic fields investigated in this work were rather modest (less than 0.40) over the location of heaviest rainfall.

Over 30% of the heavy rain samples in the eastern and southern regions were classified as pattern 4 events (Fig. 8). In contrast, less than 16% of the western events were tied to this pattern as the south-southeasterly low-level flow apparently encourages a rainshadow for heavy events in the region. The pattern 4 events show a slight summer peak in occurrence with over three-quarters observed during June, July, and August (Table 3).

Unlike the first three patterns, heavy rain totals bear a significant positive relationship with the magnitudes of most of the moisture variables (Table 2d). These positive relationships are collaborated by the finding that the mean normalized field magnitudes are markedly greater in the heavier precipitation events relative to the lighter events in the sample. Positive relationships were also found with two of the instability indices, in particular, the K index and CAPE (+). Interestingly, this is the only identified synoptic pattern in which a stability index was significantly correlated with the heavy precipitation totals. Finally, heavy rainfall amounts were related to the presence of an 850-mb warm air advection ridge and a 500-mb trough axis (i.e., maximum vorticity ridge). Negative relationships were observed with 500-mb positive vorticity advection (magnitude and ridging) and surface temperature. The negative relationship with temperature may be explained partially by the fact that the heavier events occurred more frequently in synoptic situations in which a well-defined cool sector was present to the northeast of the low pressure center (i.e., cases in which a warm front was present south of the heavy rain area). As in the first three patterns, a significant relationship was found with the diurnal timing of the event (heavier events occurring early in the morning) and the degree of veering in the lower atmosphere. Finally, precipitation totals were tied to a more southerly orientation of the mean 850–200-mb wind.

e. Pattern 5

The pattern 5 composite displays two disjunct regions of low-level convergence, one situated northwest of the composite event and the other positioned more than 400 km southeast of the event. An examination of the surface analyses connected with 20 of the events generally revealed a quiescent synoptic situation in which no well-defined surface features were found over the heavy rain area. In many events, however, a weak front was positioned in a general northwest–southeast configuration over the southeastern and northwestern sectors of the floating grid. This feature was either undergoing frontolysis or was simply not present in the immediate vicinity of the heavy rainfall. A south-southwesterly boundary layer circulation is identified in the composite; however, these winds are more southwesterly in the western Appalachian events and southerly to southeasterly in the southern and eastern events. The pattern 5 events display a slight preference for these latter regions (i.e., greater than 16%) as compared to the western region (less than 11%) (Fig. 8). Finally, well over three-quarters of the pattern 5 events are observed in June, July, and August (Table 3).

The south-southwesterly low-level flow is responsible for the warm air advection and moisture ridging, features that are observed near the heavy rain area in over two-thirds of the events. As seen in the composite, these ridges frequently intersect immediately west of the location of heaviest rainfall. The mean 850–200-mb wind is southwesterly and, unlike most of the other patterns, is not oriented parallel to any of the nearby ridging features. The normalized magnitudes of the 700-mb mixing ratio and *K* index are markedly higher over the composite grid center relative to those observed in the other fields. In fact, the mean magnitude of the mixing ratio in pattern 5 is higher than any other mean field magnitude calculated in this study.

Heavy rain totals were positively related to the magnitude of boundary layer and 850-mb θ_e convergence as well as 200-mb divergence in pattern 5. Negative relationships were found with surface temperature and the presence of ridges in the 500-mb positive vorticity advection, precipitable water, and 850-mb θ_e fields. At first glance, these relationships appear peculiar. In the case of surface temperatures, however, it is quite possible that cooler temperatures are not directly related to the heavy rain totals, but rather the cooler air is associated with a frontal boundary and its attendant clouds and precipitation, which via boundary layer convergence is positively related to the heavy rainfall totals.

Precipitation totals were most strongly related to mean 850–200-mb wind direction (more southerly winds associated with heavier precipitation) and the diurnal timing of the events (nocturnal events associated with heavier precipitation). As was the case in most of the other synoptic patterns, heavy rain totals were positively related to the degree of wind veering, a variable that corresponds closely with variables tied to an active frontal boundary (e.g., cooler temperatures, boundary layer and 850-mb θ_e convergence).

5. Summary and concluding remarks

The heavy rainfall events in this study were connected with five distinct synoptic patterns over the interior southeastern United States. All five synoptic patterns displayed relatively high normalized magnitudes of moisture (greater than 0.30 Z) and frequencies of moisture ridging (greater than 50%) over the location of heaviest rainfall. Of the seven moisture and thermodynamic fields, the 700-mb mixing ratio field displayed the highest field magnitudes and ridging frequencies in each of the synoptic patterns. Also, the ridging frequencies of 850-mb warm air advection were consistently high in each of the synoptic patterns. Warm air advection was more strongly connected with heavy rainfall than theta-e advection in each pattern. Finally, the normalized magnitudes of the *K* index were quite high relative to the other synoptic fields examined in each pattern.

The connections between heavy rainfall and various features associated with dynamic uplift (e.g., boundary layer convergence and 200-mb divergence) depended strongly on the synoptic situation. For example, 500-mb positive vorticity advection ridging was common (great-

er than 50% occurrence) in three of the synoptic situations but was observed infrequently in the remaining ones. Boundary layer convergence was common in only two of the synoptic patterns. Additionally, the normalized magnitudes of the fields associated with dynamic uplift over the heavy rain region were relatively low compared to the other investigated fields; in particular, only pattern 2 exhibited dynamic fields in which the normalized magnitudes exceeding 0.30 Z over the location of heaviest rainfall.

In three of the identified synoptic patterns, the mean 850–200-mb wind vector was oriented nearly parallel to the composite ridge axes in the moisture and 850-mb warm air advection fields. This suggests that the convective cells responsible for the heavy precipitation move and redevelop, perhaps in a train-echo pattern, along these axes where the support for convection is the greatest. This idea needs to be tested through a mesoscale analysis of the events.

Numerous statistically significant relationships were identified between heavy rainfall totals and the magnitude of various features. In all five synoptic situations, heavy precipitation totals were related to the diurnal timing of the precipitation as heavier events occurred more frequently during the nocturnal or early morning hours. This result is consistent with the findings of Crysler et al. (1982) and Winkler (1987). In three of the synoptic patterns, diurnal timing actually displayed relationships that were stronger than any of those found between the synoptic features and heavy rainfall totals.

In four of the five synoptic situations, a positive relationship was identified between precipitation totals and the degree of lower-tropospheric veering. Curiously, few significant relationships were identified between the heavy precipitation totals and the amount of moisture or the presence of moisture ridging near the location of heaviest rainfall. For example, precipitable water was positively correlated with precipitation in only two of the patterns, and no significant correlations were found with 850-mb θ_e temperature, a variable that has been related to deep convection. Only pattern 4 displayed significant relationships with many of the moisture variables. Furthermore, only pattern 4 showed significant correlations between instability (i.e., positive CAPE and *K* index) and heavy rain totals. These results indicate that while high moisture and instability are common in heavy rain events, their magnitude does not effectively discriminate extremely heavy rainfall from more modest heavy events, at least over the interior southeastern United States. Given the use of CAPE and other stability indices in assessing convective potential, it is unclear why they are not significantly correlated with the heavy rain totals in four of the five patterns. One possibility is that high values of CAPE encourage widespread convection, which in turn inhibits the moisture flux to a heavy rain-producing convective system. Also it is possible that a relationship exists, but it cannot be ascertained because of errors in the interpolation of CAPE values from the radiosonde network to the location of heaviest rainfall.

The relationships identified in this study between heavy precipitation totals and synoptic field characteristics varied strongly according to the synoptic situation. This finding underscores the idea that diagnostic indicators of extremely heavy precipitation need to be derived for common synoptic situations. Moreover, synoptic features found frequently in connection with heavy rainfall (e.g., moisture and instability) are not necessarily predictive in distinguishing an ordinary heavy rain event from an extraordinary one.

Acknowledgments. The author wishes to thank Steve Colucci and four anonymous reviewers for their helpful critiques and Becky Dobbs for the preparation of several figures. A portion of this study was supported by the National Science Foundation under Grant SES-9105628.

REFERENCES

Belville, J. D., and E. H. Goetsch, 1983: Synoptic and mesoscale considerations of a heavy rainfall event associated with warm top convection. Preprints, *Fifth Conf. on Hydrometeorology*, Tulsa, OK, Amer. Meteor. Soc., 198–205.

Bosart, L. F., and F. H. Carr, 1978: A case study of excessive rainfall centered around Wellsville, New York, 20–21 June 1972. *Mon. Wea. Rev.*, **106,** 348–362.

Chappell, C. F., 1986. Quasi-stationary convective events. *Mesoscale Meteorology and Forecasting,* P. S. Ray, Ed., Amer. Meteor. Soc., 289–310.

Crysler, K. A., R. A. Maddox, L. R., Hoxit, and B. M. Muller, 1982: Diurnal distribution of very heavy precipitation over the central and eastern United States. *Natl. Wea. Dig.,* **7,** 33–37.

Davis, R. E., and R. F. Rogers, 1992: A synoptic climatology of severe storms in Virginia. *Prof. Geogr.,* **44,** 319–32.

Doswell, C. A., H. A. Brooks, and R. A. Maddox, 1996: Flash flood forecasting: An ingredients-based methodology. *Wea. Forecasting,* **11,** 560–581.

Funk, T. W., 1991: Forecasting techniques utilized by the Forecasting Brach of the National Meteorological Center during a major convective rainfall event. *Wea. Forecasting,* **6,** 548–564.

Giordano, L. A., and J. M. Fritsch, 1983: The a-typical mid-level flow for flash floods in the mid-Atlantic states. Preprints, *Fifth Conf. on Hydrometeorology,* Tulsa, OK, Amer. Meteor. Soc., 142–148.

Grice, G. K., and G. F. Ely 1983: Surface subsynoptic and upper air analysis: An integral part of the shift routine. Preprints, *Fifth Conf. on Hydrometeorology,* Tulsa, OK, Amer. Meteor. Soc., 252–258.

——, and R. A. Maddox, 1983: Synoptic characteristics of heavy rain events in south Texas. Preprints, *Fifth Conf. on Hydrometeorology,* Tulsa, OK, Amer. Meteor. Soc., 149–155.

Heideman, K. F., and J. M. Fritsch, 1988. Forcing mechanisms and other characteristics of significant summertime precipitation. *Wea. Forecasting,* **3,** 115–130.

Holton, J. R., 1979: *An Introduction to Dynamic Meteorology.* Academic Press, 319 pp.

Hoxit, L. R., R. A. Maddox, H. M. Mogil, and F. L. Zuckerberg, 1978: Meteorological analysis of the Johnstown Pennsylvania flash flood, 19–20 July 1977. Preprints, *Second Conf. on Flash Floods: Hydrometeorological and Human Aspects,* Atlanta, GA, Amer. Meteor. Soc., 168–175.

Konrad, C. E., 1994: Moisture trajectories associated with heavy

rainfall in the Appalachian region of the United States. *Phys. Geogr.,* **15,** 227–248.

——, and S. J. Colucci, 1989: An examination of extreme cold air outbreaks over eastern North America. *Mon. Wea. Rev.,* **117,** 2687–2700.

——, and V. Meentemeyer, 1994: Lower tropospheric warm air advection patterns associated with heavy rainfall over the Appalachian region. *Prof. Geog.,* **46,** 143–155.

Korty, B., 1980: Excessive rainfall across east Texas and the lower Mississippi Valley. Preprints, *Second Conf. on Flash Floods: Hydrometeorological Aspects and Human Aspects,* Atlanta, GA, Amer. Meteor. Soc., 11–17.

Ma, K., and L. F. Bosart, 1990: A synoptic overview of a heavy rain event in southern China. *Wea. Forecasting,* **5,** 89–112.

Maddox, R. A., and C. A. Doswell, 1982: An examination of jet stream configurations, 500 mb vorticity advection and low-level thermal advection patterns during extended periods of intense convection. *Mon. Wea. Rev.,* **110,** 184–197.

——, C. F. Chappell, and L. R. Hoxit, 1979: Synoptic and meso-a scale aspects of flash flood events. *Bull. Amer. Meteor. Soc.,* **60,** 115–123.

Newton, C. W., and J. C. Fankhauser, 1975: Movement and propagation of multi-cellular convective storms. *Pure Appl. Geophys.,* **113,** 747–764.

National Climate Data Center, 1993: Radiosonde data of North America (1946–1992). Version 1.

Opitz, H. H., S. G. Summer, D. A. Wert, W. R. Synder, R. J. Kane, R. H. Brady, P. M. Stokols, and G. M. Carter, 1995: The challenge of forecasting heavy rain and flooding throughout the eastern region of the National Weather Service. Part II: Forecast techniques and applications. *Wea. Forecasting,* **10,** 91–104.

Reynolds, S. D., 1992: An excessive rainfall event caused by the remnants of a tropical cyclone, theta-e ridge, and complex terrain. NOAA Tech. Memo. NWS ER-87, National Weather Service, Washington, DC, 95–109.

SAS Institute, 1988: SAS/STAT user's guide. SAS Institute Inc., 1028 pp. [Available from SAS Institute Inc., SAS Campus Drive, Cary, NC, 27513.]

Schwartz, B. E., C. F. Chappell, W. E. Togstad, and X. P. Zong, 1990: The Minneapolis flash flood: Meteorological analysis and operational response. *Wea. Forecasting,* **5,** 3–21.

Stooksbury, D. E., and P. J. Michaels, 1991: Cluster analysis of southeastern U.S. climate stations. *Theor. Appl. Climatol.,* **44,** 143–50.

Wilson, W. H., 1992: The role of surface moisture, convergence, and 850 mb equivalent potential temperature on the formation of a flash flood producing thunderstorm. NOAA Tech. Memo. NWS ER-87, National Weather Service, Washington, DC, 121–128.

Winkler, J. A., 1987: Diurnal variations of summertime very heavy precipitation in the eastern and central United States. *Phys. Geogr.,* **8,** 210–224.

——, 1988: Climatological characteristics of summer-time extreme rainstorms in Minnesota. *Annu. Assoc. Amer. Geogr.,* **78,** 57–73.

Woodcock, F., 1980: On the use of analogues to improve regression forecasts. *Mon. Wea. Rev.,* **108,** 292–297.